Korean J. Chem. Eng., 37(8), 1346-1351 (2020)
DOI: 10.1007/s11814-020-0562-x

pISSN: 0256-1115
eISSN: 1975-7220

Enhanced Cr tolerance of perovskite oxide via $Gd_{0.1}Ce_{0.9}O_2$ surface modifications

Mingi Choi, Seoju Kim, Jaedeok Paik, and Wonyoung Lee†

Department of Mechanical Engineering, Sungkyunkwan University, Suwon 16419, Korea
(*Received 2 March 2020 • Revised 17 April 2020 • Accepted 27 April 2020*)

Abstract−Cr poisoning of the SUS interconnect and the solid oxide fuel cell electrode is one of the crucial hurdles to achieving system sustainability. Among various approaches to solving this issue, the suppression of cation segregation, especially Sr, and preventing the electrode surface from direct exposure to Cr-gas have been considered the most important factors. Herein, the effect of surface coating on mitigating Sr segregation as well as the use of strategies for protecting the electrode surface from exposure to Cr gas are discussed. Using $Sm_{0.5}Sr_{0.5}CoO_3$(SSC) as a model film electrode and $Gd_{0.1}Ce_{0.9}O_2$ (GDC) as the coating layer via a pulsed laser deposition (PLD) method, the Cr tolerance of the perovskite oxide electrode was enhanced. Electrochemical measurement at 650 °C for 200 h showed ~2.5 times higher stability of the GDC-coated SSC electrode than the bare SSC electrode. Using Auger electron spectroscopy (AES), the chemical states of the GDC-coated SSC electrode were characterized, revealing significantly reduced Sr and Cr intensity on the surface of the coated electrode when compared to the bare SSC electrode.

Keywords: Perovskite Electrode, Cr Poisoning, Sr Segregation, Surface Modification

INTRODUCTION

Solid oxide fuel cell (SOFC) is one of the cleanest energy conversion systems with the high efficiency and the high power output without any binary harmful products [1]. In particular, the development of state-of-the-art perovskite materials which can facilitate ionic and electronic conduction has allowed a higher power output at intermediate temperature (IT, <700 °C) when compared to conventional materials. In the IT ranges, Cr-composed interconnects such as SUS 430, Crofer 22 APU, and E-Brite are generally used for current collection/distribution onto the electrode owing to their compatibility at elevated temperatures, the feasibility of their use, their high electrical conductivity, and low costs [2-4]. Unfortunately, the evolution of volatile Cr gas and the occurrence of solid state intermixing between the interconnect and the electrode have been reported, both of which are known to negatively impact surface exchange reactions and the diffusivity of perovskite electrodes [5,6]. Such Cr-poisoning has been regarded as one of the most challenging hurdles to sustainable and reliable operation of SOFC systems.

Generally, state-of-the art perovskite electrodes for IT-SOFCs, such as $Sm_{0.5}Sr_{0.5}CoO_3$ (SSC), $La_{0.6}Sr_{0.4}MnO_3$ (LSM), $La_{0.6}Sr_{0.4}CoO_3$ (LSC), and $La_{0.6}Sr_{0.4}Co_{0.2}Fe_{0.8}O_3$ (LSCF) are reported to be vulnerable to Cr poisoning [5-8]. The vulnerability of those materials to Cr-poisoning is firstly facilitated by the Sr segregation, forming the Sr-O terminated surface at the perovskite surface [8-10]. Since the Cr gas species is easily adsorbed onto the Sr-terminated perovskite surface, the formation of secondary phase clusters such as $SrCrO_4$ tends to occur near the Sr terminal [5,11]. These secondary phases substantially reduce the electrical performance and surface exchange reaction rates of the electrode, resulting in significant performance degradation over operating time [5,10,12-16].

To prevent Cr poisoning of the perovskite oxide electrode, several efforts have been suggested to avoid the direct exposure of the perovskite surface to Cr-gas species [3,7,12,17,18]. Recently, a coating of sacrificing layer with spinel materials at the interconnect has been investigated. Because those Fe-, Co-, Ni-, and Cu-based spinel structures have the several advantages such as adequate conductivity, similar coefficient of thermal expansion (CTE), and chemical stability, a substantial improvement in electrochemical stability was reported by reducing the Cr-poisoning onto the perovskite surface [17]. However, since the role of these spinel coating layers is limited to prevent the perovskite surface to exposure of Cr-gas species, the Sr segregation and the formation of secondary phase clusters still remain as the significant cause for the chemical degradation of the electrode performance. Therefore, a way to prevent the electrode from both direct exposure to Cr gas and Sr segregation should be further investigated.

We speculated that conformal coating onto the perovskite oxide with certain material, which can achieve resistivity to Cr gas and suppression of Sr segregation, is one of the rational strategies to suppress Cr-poisoning. Therefore, two major points were considered to prevent Cr-poisoning. One is to suppress the Sr segregation to inhibit the formation of the Sr-O terminated surface which is vulnerable to Cr-poisoning. The other is to prevent the direct exposure of Cr-gas species by using a Cr-resistant material. Recently, a conformal coating that contains fluorite material such as CeO_2 and ZrO_2 demonstrated remarkable suppression of Sr toward the surface, leading to a notable increase in the stability of the perovskite electrode [19,20]. With a coating material which has less oxygen vacancy concentration, the electrostatic attraction between the enriched oxygen vacancy at the surface ($V_o^{\cdot\cdot}$) and the doped-Sr (Sr'_{Ln}), which is one of the crucial drivers to attract the doped-Sr toward the surface, could be minimized [19,21-23]. In the view of the expo-

†To whom correspondence should be addressed.
E-mail: leewy@skku.edu

sure of Cr-gas species onto the perovskite surface, Li et al. reported that the conformal surface coating of perovskite oxide with Cr-resistant material such as La_2NiO_4 and $PrNi_{0.5}Mn_{0.5}O_3$ demonstrated increased stability owing to the protection of perovskite surface to the Cr gas species [6,7]. Since fluorite materials such as CeO_2 and ZrO_2 have a high tolerance to Cr adsorption and reactivity, they could be considered as a coating material to prevent the perovskite surface. Therefore, further investigation of the coating layer with considering those comprehensive factors should be conducted.

In this study, we report the improved electrochemical stability of perovskite oxide electrodes from the Cr-poisoning with surface coating. Using pulsed laser deposition (PLD), we deposited the SSC film as a model film cathode, and $Gd_{0.1}Ce_{0.9}O_2$ (GDC) film was coated onto the surface of SSC film. We speculated that since GDC has ~3-fold lower oxygen vacancy concentration than SSC, it can reduce the electrostatic driver of Sr segregation near the surface of SSC. Furthermore, since GDC has much less reactivity with Cr-gas species than SSC, we speculated that conformal GDC layer can prevent the SSC film surface from the exposure to the Cr-gas species. Electrochemical impedance spectra (EIS) measurement for long-term operation was assessed at 650 °C for 200 h with Cr_2O_3 powder to provide the volatile Cr-gas species. SSC film without GDC coating showed rapid performance degradation, 4-fold higher R_p after 200 h than that of 0 h. In contrast, GDC coated SSC film showed ~1.5 times larger R_p value at 200 h compared to that at 0 h, representing ~2.5 times higher electrochemical stability than SSC film. Especially, Auger electron spectroscopy (AES) measurement further revealed the significantly reduced Sr segregation, and the reduced amount of Cr-species at the GDC coated SSC film, indicating the effective protection of SSC surface with the presence of GDC coating layer. Moreover, the surface coverage of Cr-species was greatly reduced in GDC coated SSC film (~6.9%) than SSC film without GDC coating (~29%). Therefore, we conclude that Cr-tolerance of perovskite surface can be greatly enhanced with GDC coating through the reduction of the Sr segregation and protection of the SSC surface from the direct exposure Cr-gas species.

EXPERIMENTAL DETAILS

1. Thin Film Fabrication

Stoichiometric powders of $Sm_{0.5}Sr_{0.5}CoO_{3-\delta}$ (SSC) and $Gd_{0.1}Ce_{0.9}O_{2-\delta}$ (GDC) were prepared via the glycine-nitrate process. High purity $Sm(NO_3)_3{\cdot}6H_2O$ (99.999%, Sigma Aldrich, USA), $Sr(NO_3)_2$ (99.995%, Sigma Aldrich, USA), $Co(NO_3)_2{\cdot}6H_2O$ (99%, Sigma Aldrich), $Gd(NO_3)_3{\cdot}6H_2O$ (99.9%, Sigma Aldrich, USA), $Ce(NO_3)_3{\cdot}6H_2O$ (99%, Sigma Aldrich, USA), and glycine (99%, Daejung, Republic of Korea) were dissolved in distilled water to form aqueous mixed solution. The solutions were boiled on a hot plate for 3 h for gelation. After combustion in the heated ceramic pot, the resultant powder was dry-milled for 24 h. The dried powder was calcined for phase formation at 800 °C for 3 h. Then, the powder was pressed at 40 MPa and calcined at 1,200 °C to form dense disk-like pellets. Using pulsed laser deposition (PLD), the model films were symmetrically deposited onto both sides of a 8 mol% single crystal Y_2O_3-stabilized ZrO_2 (YSZ) substrate (100) (MTI:G160103) with a thickness of 500 μm. Deposition conditions of PLD were as below: 110 mJ of laser power per pulse at 5 Hz, a substrate temperature of 700 °C, and an oxygen partial pressure of 50 mTorr. The symmetrically deposited cells were slowly cooled to room temperature at an oxygen pressure of 10 Torr for 2 h for oxide phase formation.

2. Characterizations

X-ray diffraction (XRD; X'Pert-Pro MRD, PANalytical) with Cu

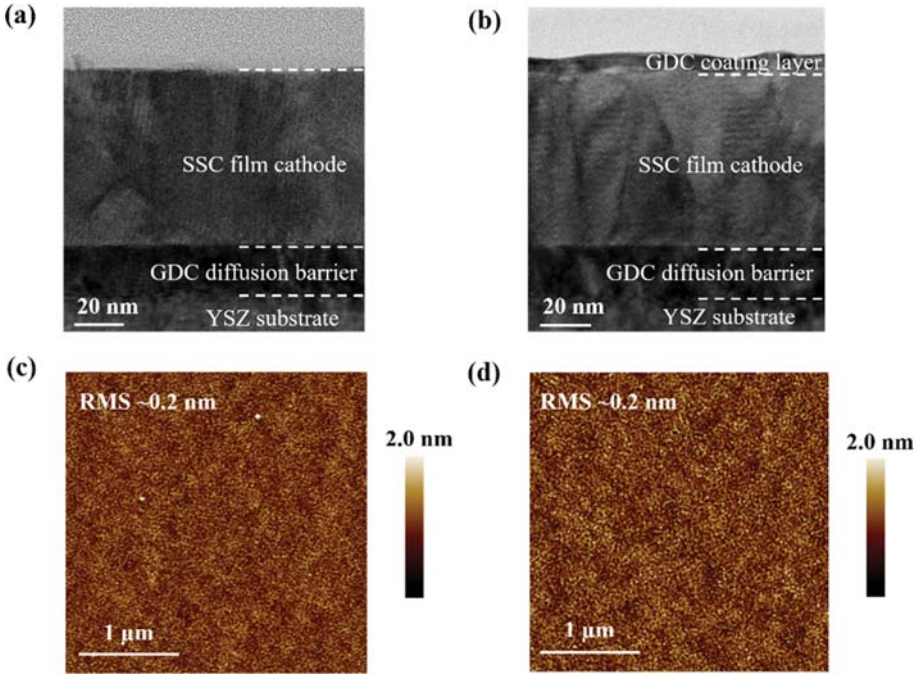

Fig. 1. Cross sectional TEM images of (a) SSC film, and (b) GDC/SSC film, and AFM images of (c) SSC film, and (d) GDC/SSC film of as-deposited films.

Kα (λ=1.5406 Å) was employed at room temperature for characterizing the crystal structures of thin films. The morphology of the thin film surfaces was characterized using atomic forced microscopy (AFM, Multimode 8 AFM, Nanoscope V) and scanning electron microscopy (SEM, JSM7000F, JEOL). A transmission electron microscope (TEM, JEM ARM200F, JEOL) was used to characterize the cross-sectional view of thin films. The auger electron spectroscopy (AES, PHI 700, ULVAC-PHI) was used to identify the surface cation content. Electrochemical impedance spectroscopy (EIS) data were measured at 650 °C in ambient air at a frequency range of 10^{-2}-10^{6} Hz with an impedance analyzer (GAMRY Reference 600, GAMRY Inc.). 20 g of Cr_2O_3 powder was placed near samples to provide the Cr-atmosphere when EIS evaluation was assessed.

RESULTS AND DISCUSSION

To evaluate the change of R_p value in a Cr atmosphere, thin film model electrodes were fabricated via PLD. On a (100) YSZ substrate, the GDC layer was deposited as a diffusion barrier at a thickness of ~27 nm to avoid the formation of $SrZrO_3$ at the interfaces between the YSZ and the SSC layers [24]. Thereafter, the SSC layer was deposited as an electrode at a thickness of ~88 nm, as shown in Fig. 1(a). To compare the effect of coating layer onto the perovskite film surface, a GDC layer was additionally deposited at a thickness of ~6.5 nm onto the SSC film, as shown in Fig. 1(b). The sample without and with GDC layer in Fig. 1(a)-(b) are denoted as SSC film and GDC/SSC film, respectively. As shown in AFM images of Fig. 1(c)-(d), as-deposited SSC film and GDC/SSC film show smooth surface morphology with a root-mean-square (RMS) roughness of ~0.2 nm. In particular, GDC layer covered the entire SSC surface without open surface which can be poisoned by the Cr-gas species. XRD patterns in Fig. S1 show that both samples were epitaxially grown along the lattice direction of YSZ (100). Moreover, XRD patterns of SSC film and GDC/SSC film (See Fig. S1(b)) show the same peak position at the SSC (200), representing no noticeable strain effect on the coated SSC film due to the presence of the top GDC coating layer. Therefore, we can conclude that effects from the structural difference such as roughness, different lattice orientation, and open pores can be neglected.

EIS measurements were performed at 650 °C for 200 h to reveal the effect of GDC layer on protecting the SSC surface from Cr-poisoning. Cr_2O_3 powders were located near the samples to provide the Cr-gas species. In general, the degradation rate is significantly accelerated because the thin-film configured electrode is substantially weak to the chemical stability at the elevated temperature [10,20]. In Fig. 2(a), the SSC film shows rapid increase in polarization resistance (R_p), resulting in ~4 times larger R_p value at 200 h compared to the initial R_p value at 0 h. GDC/SSC film shows a slightly higher initial R_p value at 0 h than that of SSC film because GDC has relatively lower oxygen surface exchange rate than SSC for ORR [19]. Interestingly, despite the lower oxygen surface exchange rate of GDC than that of SSC, the initial R_p value of GDC/SSC film is comparable to that of SSC film. Similar to our results, several reports have demonstrated that coated perovskite electrodes with less reactive materials such as ZrO_2/LSC, CeO_2/LSCF, and LSM/LSCF showed comparable initial ORR kinetics to the non-coated perovskite electrode [19,20,25]. The detrimental effects of the coating layers on the ORR kinetics may be insignificant when the layer thickness is sufficiently thin. Therefore, the thickness of the coating layer should be optimized considering both the stability and the initial performance. On the other hand, GDC/SSC film shows the ~1.5 times larger R_p value at 200 h compared to that at 0 h. Hence, GDC/SSC film represents the ~2.5 times higher electrochemical stability than SSC film.

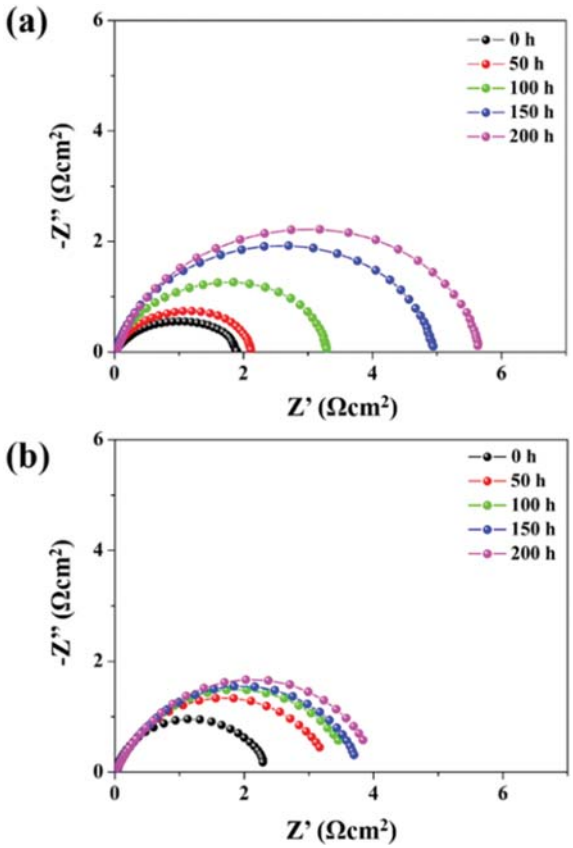

Fig. 2. Changes in the R_p value of (a) SSC and (b) GDC/SSC film with exposure to Cr gas species at 650 °C for 200 h.

Fig. 3 displays the surface morphology of both SSC and GDC/SSC film at as-deposited state, and after operating at 650 °C for 200 h under dry air and Cr-gas. Surface morphology of the as-deposited samples by SEM in Figs. 3(a) and (d) has no discernible clusters with clean surface in accordance with AFM images in Figs. 1(c)-(d). However, after operating at 650 °C for 200 h, secondary clusters are generated. Since Sr-doped perovskite oxides generally suffer from the Sr segregation and subsequent secondary phase formation at the surfaces, these secondary clusters may be related to the Sr-enriched secondary phases such as SrO_x and $Sr(OH)_x$ [26]. In Fig. 3(b), SSC film after operating at 650 °C for 200 h under dry air shows secondary clusters with a width of 200-300 nm. In the case of under Cr-gas species (See Fig. 3(c)), those clusters grow and form a bigger cluster width, the width of ~2 μm. It is attributed to the fact that the generation of secondary cluster is more facilitated under Cr-gas species compared to that under dry air [8]. Whereas, in Fig. 3(e)-(f), the generation of such clusters in GDC/SSC film is

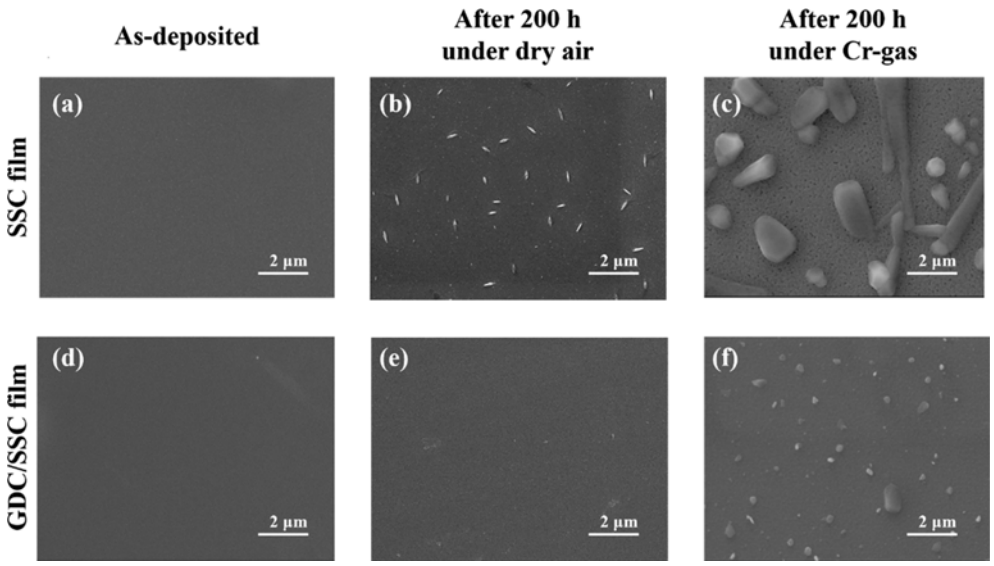

Fig. 3. SEM images of the SSC film and the GDC/SSC film under dry air and Cr-gas. SSC film at (a) as-deposited state, after operating for 200 h (b) under dry air, and (c) under Cr-gas. GDC/SSC film at (d) as-deposited state, after operating for 200 h (e) under dry air, and (f) under Cr-gas.

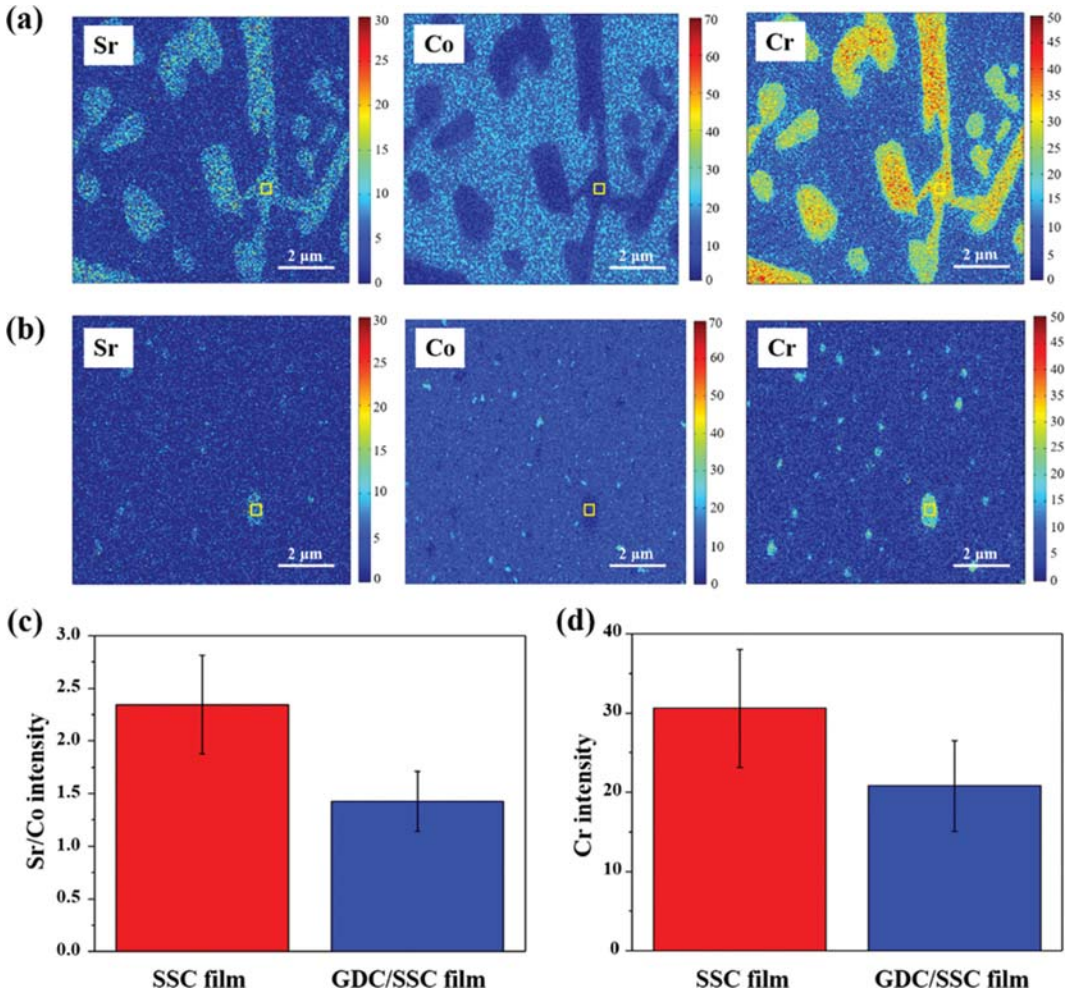

Fig. 4. Chemical characterization of generated clusters by AES. AES mapping of Sr, Co, and Cr in (a) SSC film and (b) GDC/SSC film after 200 h. Quantified values of (c) Sr/Co ratio and (d) Cr intensity obtained in AES mapping.

significantly suppressed. Under dry air (See Fig. 3(e)), it shows no discernible secondary clusters, representing the significantly suppressed Sr segregation with GDC layer. According to Chen et al., it is due to the reduced electrostatic driver (i.e., oxygen vacancy, normal charge of +2), which attracts the doped-Sr (i.e., normal charge of −1), with the surface coating of CeO_2 layer (GDC in here) [19]. Under Cr-gas in Fig. 3(f), it represents the substantial generation of secondary cluster with the width of 0.77-2.5 μm. However, the size of those clusters and surface coverage is significantly suppressed compared to that in SSC film (See Fig. 3(c)), which is in accordance with the higher electrochemical stability of GDC/SSC film in Fig. 2.

To verify the chemical composition of generated secondary clusters at the surface of each film, we performed AES analysis. Fig. 4(a) shows the elemental mapping of the SSC film after operation at 650 °C for 200 h under Cr-gas species, revealing that generated secondary clusters are predominantly composed of Sr and Cr. Thus, we could verify that the generated clusters are formed with $SrCrO_4$ in an accordance with reported papers [5,11]. It has been reported that the formation of Sr-enriched secondary clusters is more pronounced under Cr-atmosphere than pure ambient air because the formation enthalpy of $SrCrO_4$ is much lower than that of SrO ($\Delta_f H^o_{SrCrO_4}$=−1,439 kJ/mol, $\Delta_f H^o_{SrO}$=−592 kJ/mol at 298.15 K) [27]. Cr-gas species are adsorbed onto the as-segregated Sr clusters, thereby forming $SrCrO_4$. Under Cr-atmosphere, generation and agglomeration of such clusters are more facilitated compared to that under pure ambient air, despite the same operating temperature and time. In Fig. 4(b), Sr/Cr-composed clusters also appear on the GDC/SSC film as similar with SSC film, whereas the intensity is significantly reduced. As shown in Fig. 4(c)-(d), to compare the degree of Sr segregation and Cr intensity of both samples, we quantitatively extracted the Sr/Co ratio, which is the general factor to show the Sr segregation and Cr concentration present on the film; a scan area of 300×300 nm^2 was established in both the SSC and GDC/SSC films [10]. The intensity of Sr/Co and Cr in GDC/SSC film is ~1.6-fold and ~1.5-fold lower than that in SSC film, respectively, indicating the significantly suppressed Sr segregation and Cr adsorption with GDC coating. As well as the chemical intensity, we calculated the surface coverage of the secondary clusters through the image analysis, showing the ~29 and 6.9% in the SSC and the GDC/SSC film, respectively. Thus, it can be ascribed that rapid increase in the R_p of the SSC film is owing to the retarded surface exchange reactions including the surface adsorption, dissociation, and charge transfer because of considerable generation of secondary clusters on the surface of the film via Cr-poisoning [26]. In addition, Sr-enriched layers near the outermost surface due to the Sr segregation substantially destroy the initial stoichiometry, lowering the ORR kinetics [9,28,29]. Therefore, the destructed stoichiometry of uncovered surface could be another reason for the significantly increased R_p despite only 29% surface coverage of secondary clusters. On the other hand, GDC/SSC film have significant effect in reducing the Cr-poisoning, resulting in smaller clusters and smaller surface coverage in accordance with substantially maintained R_p over 200 h. Interestingly, as well as Sr and Cr, a small amount of Co particles is also observed, indicating that Co segregation also occurred with Sr segregation. However, since Cr tends to adsorb selectively onto the Sr rather than the Co, the major cluster is predominantly composed of Sr and Cr [5,8]. Therefore, we can conclude that the GDC coating layer onto the SSC film significantly suppresses the Sr segregation and the subsequent generation of $SrCrO_4$ compared to the SSC film without GDC coating layer. Furthermore, since conformal GDC coating layer has high resistivity to the Cr-gas species than the SSC film, it could avoid the undesirable chemical degradation at the surface and Cr-poisoning through the open surface.

The increased Cr-tolerance with the GDC layer can be attributed to two major aspects. The first is suppression of Sr segregation. The perovskite oxide surface suffers Cr-poisoning more severely when the surface is enriched with Sr because of the preferential adsorption of Cr on the Sr-terminated surface. However, it could be prevented by the presence of a surface coating layer, resulting in higher electrochemical and chemical stability. Furthermore, for a rational design of the surface coated electrode, various aspects based on our results should be considered, including the chemical stability of the designed-film with respect to the suppression of Sr segregation, the phase stability of the coated film under the Cr-atmosphere, and the physical stability at the interface without delamination as shown in Fig. 5. For suppression of Sr segregation, the coating layer should minimize the drivers, which promotes cation segregation toward the surface. For example, because enriched oxygen vacancy at the surface can induce Sr segregation toward the surface, the coating layer should have less amount of oxygen vacancy than the

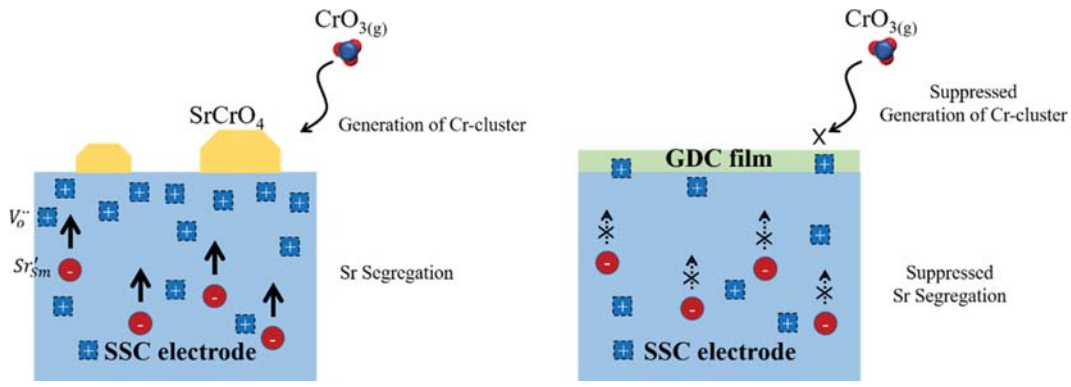

Fig. 5. Schematic overview for rational design of a coating layer against Cr-poisoning.

perovskite film. Since GDC has ~3-fold less oxygen vacancy concentration than SSC ($[V_o^{\cdot\cdot}/O_o^{\times}]$ ~0.049 for GDC, and $[V_o^{\cdot\cdot}/O_o^{\times}]$ ~0.142 for SSC), it may reduce the electrostatic driver of Sr segregation at the surface of perovskite oxide [30]. In addition, the strain effect between the coating layer and the perovskite film can be an another major designing factor [9,29]. Thus, the lattice mismatch which generates the tensile or compressive strain between the two films should be considered to avoid facile cation segregation. In this study, the strain effect between the GDC and the SSC films is negligible. Phase stability of the coating material under Cr-atmosphere should be guaranteed because it can cause other deteriorative effects on electrochemical performance. As shown in Fig. S2, despite long-term operation in Cr-atmosphere, it did not show GDC related Cr clusters, confirming its phase stability under Cr-atmosphere. Lastly, physical stability should be considered for a robust electrode. Since the thermal expansion coefficient value is similar between GDC (12.5×10^{-6}/K) and the SSC (20.5×10^{-6}/K), it did not show delamination after operation. Therefore, careful consideration for material properties is required to apply the coating layer for preventing Cr-poisoning.

CONCLUSIONS

To prevent the SSC surface from Cr-poisoning, a GDC layer was coated onto the SSC electrode. With the GDC/SSC film electrode, electrochemical stability was significantly improved, resulting in ~2.5 times higher stability at 650 °C for 200 h compared to SSC film electrode without GDC coating. Using SEM characterization, we could observe decreased growth of secondary clusters and surface coverage in GDC/SSC film. Furthermore, AES analysis confirmed that notable suppression of Sr segregation and Cr adsorption had occurred on the GDC/SSC film compared to the SSC film, which is in accordance with the higher electrochemical stability of GDC/SSC film measured by EIS. Therefore, we conclude that Cr-poisoning can be overcome with the rational design of a coating layer and material selection which can satisfy the requirements for protection from the Cr-poisoning.

ACKNOWLEDGEMENTS

This work was supported by the Korea Institute of Energy Technology Evaluation and Planning (KETEP) and the Ministry of Trade, Industry & Energy (MOTIE) of the Republic of Korea (No. 20173010032170).

SUPPORTING INFORMATION

Additional information as noted in the text. This information is available via the Internet at http://www.springer.com/chemistry/journal/11814.

REFERENCES

1. E. D. Wachsman and K. T. Lee, *Science*, **334**, 935 (2011).
2. Z. Yang, K. S. Weil, D. M. Paxton and J. W. Stevenson, *J. Electrochem. Soc.*, **150**, A1188 (2003).
3. E. Zanchi, B. Talic, A. Sabato, S. Molin, A. Boccaccini and F. Smeacetto, *J. Eur. Ceram. Soc.*, **39**, 3768 (2019).
4. P. Y. Hou, K. Huang, W. T. Bakker, *ECS Proceedings Volumes*, **1999**, 737 (1999).
5. N. Ni, S. J. Cooper, R. Williams, N. Kemen, D. W. McComb and S. J. Skinner, *ACS Appl. Mater. Interfaces*, **8**, 17360 (2016).
6. Y. Chen, S. Yoo, X. Li, D. Ding, K. Pei, D. Chen, Y. Ding, B. Zhao, R. Murphy and B. Deglee, *Nano Energy*, **47**, 474 (2018).
7. J. Li, J. Li, D. Yan, J. Pu, B. Chi and L. Jian, *Electrochim. Acta*, **270**, 294 (2018).
8. B. Wei, M. Schroeder and M. Martin, *ACS Appl. Mater. Interfaces*, **10**, 8621 (2018).
9. W. Lee, J. W. Han, Y. Chen, Z. Cai and B. Yildiz, *J. Am. Chem. Soc.*, **135**, 7909 (2013).
10. J. Y. Koo, H. Kwon, M. Ahn, M. Choi, J.-W. Son, J. W. Han and W. Lee, *ACS Appl. Mater. Interfaces*, **10**, 8057 (2018).
11. T. Horita, Y. Xiong, H. Kishimoto, K. Yamaji, M. E. Brito and H. Yokokawa, *J. Electrochem. Soc.*, **157**, B614 (2010).
12. S. Geng, Y. Pan, G. Chen and F. Wang, *Int. J. Hydrogen Energy*, **44**, 9400 (2019).
13. Y. Chen, W. Jung, Z. Cai, J. J. Kim, H. L. Tuller and B. Yildiz, *Energy Environ. Sci.*, **5**, 7979 (2012).
14. W. Jung and H. L. Tuller, *Energy Environ. Sci.*, **5**, 5370 (2012).
15. Y. Li, W. Zhang, Y. Zheng, J. Chen, B. Yu, Y. Chen and M. Liu, *Chem. Soc. Rev.*, **46**, 6345 (2017).
16. D. Kim, J. W. Park, B.-H. Yun, J. H. Park and K. T. Lee, *ACS Appl. Mater. Interfaces*, **11**, 31786 (2019).
17. M. Zhao, S. Geng, G. Chen and F. Wang, *J. Power Sources*, **414**, 530 (2019).
18. N. Demeneva, O. Kononenko, D. Matveev, V. Kharton and S. Bredikhin, *Mater. Lett.*, **240**, 201 (2019).
19. H. Chen, Z. Guo, L. A. Zhang, Y. Li, F. Li, Y. Zhang, Y. Chen, X. Wang, B. Yu and J.-m. Shi, *ACS Appl. Mater. Interfaces*, **10**, 39785 (2018).
20. Y. Wen, T. Yang, D. Lee, H. N. Lee, E. J. Crumlin and K. Huang, *J. Mater. Chem. A*, **6**, 24378 (2018).
21. N. Tsvetkov, Q. Lu, L. Sun, E. J. Crumlin and B. Yildiz, *Nat. Mater.*, **15**, 1010 (2016).
22. D. Kim, R. Bliem, F. Hess, J.-J. Gallet and B. Yildiz, *J. Am. Chem. Soc.*, **7**, 3548 (2020).
23. F. Hess and B. Yildiz, *Phys. Rev. Mater.*, **4**, 015801 (2020).
24. K. Chen, N. Li, N. Ai, M. Li, Y. Cheng, W. D. Rickard, J. Li and S. P. Jiang, *J. Mater. Chem. A*, **4**, 17678 (2016).
25. M. E. Lynch, L. Yang, W. Qin, J.-J. Choi, M. Liu, K. Blinn and M. Liu, *Energy Environ. Sci.*, **4**, 2249 (2011).
26. Z. Cai, M. Kubicek, J. r. Fleig and B. Yildiz, *Chem. Mater.*, **24**, 1116 (2012).
27. K. Jacob and K. Abraham, *J. Phase Equilib.*, **21**, 46 (2000).
28. J. Druce, H. Tellez, M. Burriel, M. Sharp, L. Fawcett, S. Cook, D. McPhail, T. Ishihara, H. Brongersma and J. Kilner, *Energy Environ. Sci.*, **7**, 3593 (2014).
29. B. Koo, H. Kwon, Y. Kim, H. G. Seo, J. W. Han and W. Jung, *Energy Environ. Sci.*, **11**, 71 (2018).
30. M. Choi, I. A. M. Ibrahim, K. Kim, J. Y. Koo, S. J. Kim, J.-W. Son, J. W. Han and W. Lee, *ACS Appl. Mater. Interfaces*, **12**, 21494 (2020).

Supporting Information

Enhanced Cr tolerance of perovskite oxide via $Gd_{0.1}Ce_{0.9}O_2$ surface modifications

Mingi Choi, Seoju Kim, Jaedeok Paik, and Wonyoung Lee†

Department of Mechanical Engineering, Sungkyunkwan University, Suwon 16419, Korea
(*Received 2 March 2020 • Revised 17 April 2020 • Accepted 27 April 2020*)

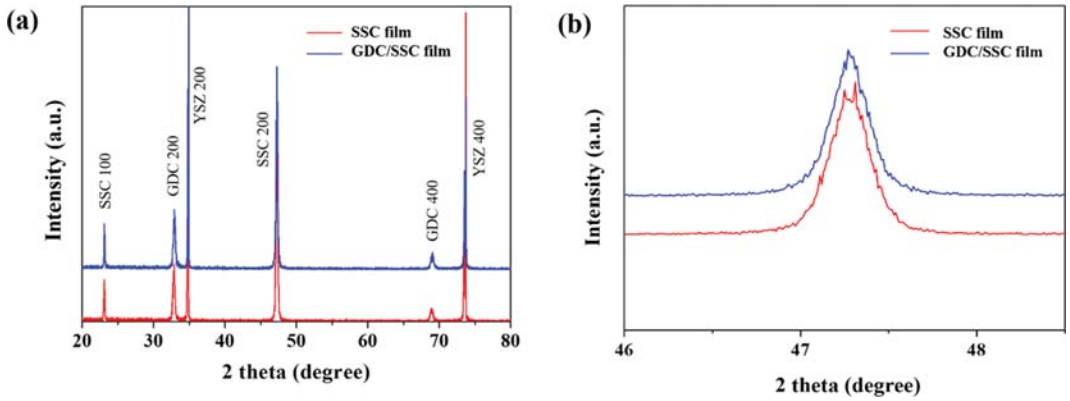

Fig. S1. XRD patterns of SSC film and GDC/SSC film. (a) full range, and (b) SSC (200) range.

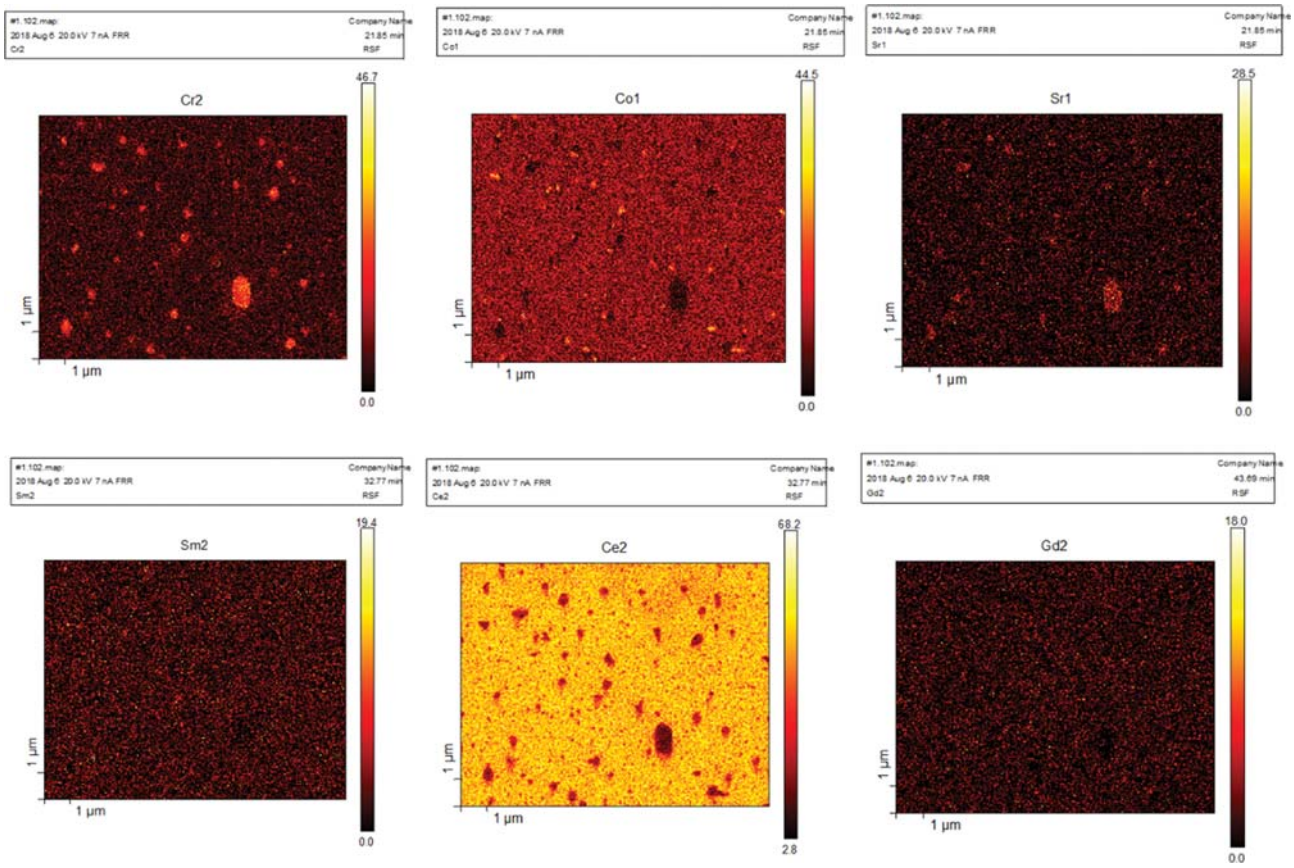

Fig. S2. AES mapping of GDC/SSC film after operating at 650 °C for 200 h.